University Library

MINERVA ACCESS

A gateway to Melbourne's research publications

Minerva Access is the Institutional Repository of The University of Melbourne

Author/s:
Wan, Y;Samundsett, C;Bullock, J;Hettick, M;Allen, T;Yan, D;Peng, J;Wu, Y;Cui, J;Javey, A;Cuevas, A

Title:
Conductive and Stable Magnesium Oxide Electron-Selective Contacts for Efficient Silicon Solar Cells

Date:
2017-03-08

Citation:
Wan, Y., Samundsett, C., Bullock, J., Hettick, M., Allen, T., Yan, D., Peng, J., Wu, Y., Cui, J., Javey, A. & Cuevas, A. (2017). Conductive and Stable Magnesium Oxide Electron-Selective Contacts for Efficient Silicon Solar Cells. Advanced Energy Materials, 7 (5), https://doi.org/10.1002/aenm.201601863.

Persistent Link:
https://hdl.handle.net/11343/292143

Article type: Full Paper

Conductive and Stable Magnesium Oxide Electron-Selective Contacts for Efficient Silicon Solar Cells

Yimao Wan, Chris Samundsett, James Bullock, Mark Hettick, Thomas Allen, Di Yan, Jun Peng, Yiliang Wu, Jie Cui, Ali Javey, and Andres Cuevas*

Dr. Yimao Wan, Chris Samundsett, Thomas Allen, Di Yan, Jun Peng, Yiliang Wu, Dr. Jie Cui, and Prof. Andres Cuevas

[1] Research School of Engineering, The Australian National University (ANU), Canberra, ACT 0200, Australia

(Email: yimao.wan@anu.edu.au)

Dr. James Bullock, Mark Hettick, Prof. Ali Javey

[2] Department of Electrical Engineering and Computer Sciences, University of California, Berkeley, California 94720, USA.

Keywords: solar cell, magnesium oxide, electron-selective contact

This is the author manuscript accepted for publication and has undergone full peer review but has not been through the copyediting, typesetting, pagination and proofreading process, which may lead to differences between this version and the Version of Record. Please cite this article as doi: 10.1002/aenm.201601863.

This article is protected by copyright. All rights reserved.

Author Manuscript

Author Manuscript

Abstract

A high Schottky barrier (> 0.65 eV) for electrons is typically found on lightly doped *n*-type crystalline (c-Si) wafers for a variety of contact metals. This behaviour is commonly attributed to the Fermi-level pinning effect and has hindered the development of *n*-type c-Si solar cells, whilst its *p*-type counterparts have been commercialised for several decades, typically utilising aluminium alloys in full-area, and more recently, partial-area rear contact configurations. Here we demonstrate a highly conductive and thermally stable electrode composed of a magnesium oxide / aluminium (MgO_x/Al) contact, achieving moderately low resistivity Ohmic contacts on lightly doped *n*-type c-Si. The electrode, functionalized with nanoscale MgO_x films, significantly enhances the performance of *n*-type c-Si solar cells to a power conversion efficiency of 20%, advancing *n*-type c-Si solar cells with full-area dopant-free rear contacts to a point of competitiveness with the standard *p*-type architecture. The low thermal budget of the cathode formation, its dopant-free nature, and the simplicity of the device structure enabled by the MgO_x/Al contact open up new possibilities in designing and fabricating low-cost optoelectronic devices, including solar cells, thin film transistors or light emitting diodes.

1 Introduction

Crystalline silicon (c-Si) has been dominating worldwide photovoltaic (PV) production for decades, with a global market share of around 90%, making it unequivocally

This article is protected by copyright. All rights reserved.

the most important PV technology nowadays. The majority of commercialised c-Si PV devices are based on a simple solar cell architecture—a *p*-type c-Si wafer with a front phosphorus diffusion and a full-area aluminium (Al) alloyed rear back surface region. The success of this architecture is largely due to the simple, low-cost formation of a highly doped p^+ region upon alloying, which leads to a low contact resistance for hole transport and a reasonable level of recombination suppression at the rear surface. When Al is directly deposited on *n*-type c-Si, however, and even if it is not alloyed with the silicon, the contact behaves in a rectifying fashion and is associated with a high contact resistance, despite the small difference (~0.1–0.2 eV) that exists between the Al work function and the electron affinity of silicon and the consequently low barrier height predicted by the Schottky-Mott rule.[1,2] This behaviour is widely attributed to the Fermi-level pinning phenomenon, induced by a high density of bandgap states or defects at the metal/semiconductor interfaces, which leads to a relatively high Schottky barrier height (Φ_B) of ~0.65 eV that hinders the flow of electrons out of the *n*-type silicon wafer.[1,2]

The approaches for addressing this problem can be inferred by looking into the dependence of contact resistivity ρ_c, on the Schottky barrier height Φ_B, and the surface doping concentration of the semiconductor N_d, which is given by $\rho_c \propto \exp\left(\frac{\Phi_B}{\sqrt{N_d}}\right)$. Historically, an Ohmic contact to *n*-type silicon wafers has been achieved by means of heavy phosphorus doping at the surface of the solar cells (i.e., increasing N_d) via thermal diffusion or plasma-assisted deposition. Despite its success in producing record-efficiency silicon solar cells, doping usually creates process complexity and requires a high temperature, in excess of 800 ^{o}C for the thermal diffusion of dopants[3] or for the re-crystallization of deposited silicon

Author Manuscript

This article is protected by copyright. All rights reserved.

layers.[4] Noxious gasses are normally used in silicon heterojunction solar cell technology to introduce dopants in hydrogenated amorphous silicon layers deposited by PECVD.[5]

Another obvious approach to reducing ρ_c is to reduce Φ_B. One straightforward technique to reduce Φ_B for electron transport is the utilization of a metal layer with a very low work function, such as calcium[6] and magnesium,[7-10] resulting in a relatively low barrier height of ~0.35 eV on *n*-type c-Si.[2,7] An alternative, or complementary, technique is the de-pinning of the Fermi-level by inserting an interfacial layer between the outer metal electrode and the inner silicon absorber. The interlayer functions as a passivating layer to reduce the density of states/defects at the metal/silicon interface while being conductive enough to allow significant transport of carriers through it. Several properties of the interlayer are desirable for achieving a low contact resistivity: (*i*) low conduction band offset to c-Si, (*ii*) low tunnelling effective mass, (*iii*) low bulk resistivity, and (*iv*) possible capability of reducing the work function of the outer metal layer.

Based on abovementioned implications, extensive efforts have been devoted to explore materials to form electron-selective contacts on *n*-type c-Si wafers without intentional dopants. Materials such as alkali/alkaline earth metal salts and carbonates (e.g., lithium fluoride,[11-13] magnesium fluoride,[14] and caesium carbonate[15,16]) and transition metal oxides (e.g., titanium oxide[17,18]) have been reported to enhance significantly the Ohmic contact of Al to *n*-type c-Si, enabling the power conversion efficiency of silicon solar cells to reach about 20%.

Another candidate which has been shown to have promise in light-emitting diodes[19] but without much development in solar cells is magnesium oxide (MgO_x). Stoichiometric

This article is protected by copyright. All rights reserved.

Author Manuscript

MgO_x (x=1) is well-known to be an insulator with a wide energy band gap.[20] Recently, MgO_x has been reported to suppress the recombination loss within a titania compact layer in perovskite solar cells.[21,22] To our knowledge, however, the application of those oxides as electron-selective contacts to *n*-type c-Si has not been explored. In this work, we develop a conductive and thermally stable electron-selective contact on *n*-type c-Si facilitated by a nanoscale MgO_x film. We investigate the electronic band structure and conduction properties of the thermally evaporated MgO_x/Al electron-selective contacts. The electron contact is then applied to the full rear surface of *n*-type silicon solar cells, for the first time with this material, achieving a fill factor of 80.5% and a power conversion efficiency of 20%. Finally, the devices featuring the MgO_x/Al contact are shown to be thermally stable upon annealing at a temperature of up to 400 °C for 40 minutes.

2 Results and Discussion

MgO_x films were thermally evaporated at a rate of 0.2 Å/s from a 4N–purity MgO_x powder source, with a base pressure of $< 2 \times 10^{-6}$ mbar. X-ray diffraction measurements showed that the evaporated MgO_x thin films have an amorphous structure without any observable peaks, in contrast with the MgO_x powder, which has distinctive diffraction peaks (see supporting information S1a). The electronic band structure was characterized via X-ray photoelectron spectroscopy (XPS), using monochromatic Al Kα X-rays with a photon energy of 1486.7 eV at a pressure in the range of 10^{-9} to 10^{-10} mbar. Figure 1 shows the XPS measurement results, including (a) core levels of Mg 1s, (b) core levels of O 1s, (c) the valence band region, and (d) secondary electron cut-off work function measurement of the MgO_x/Al interface. While the Mg 1s spectra exhibits a typical peak at ~1304 eV, the core

Author Manuscript

This article is protected by copyright. All rights reserved.

level of O 1s can be split into the oxide O^{2-} and peroxide O_2^{2-} doublet peaked at 529.8 eV and 531.5 eV, respectively, as ascribed in previous work.[23] Extraction of the MgO_x film stoichiometry based on core level peak areas shows the thermally evaporated MgO_x to be more metallic, with an O to Mg atomic fraction of 0.75, significantly lower than the stoichiometry of the powder source, found to be 0.95 (see supporting information S1d). Note that the sample for core level analysis has a bare MgO_x layer (i.e., it does not have an Al over-layer), and hence the stoichiometry may not be representative of the layer affected by aluminium deposition in the final contacts.

We now turn to the discussion of the valence band spectrum of the MgO_x films shown in Figure 1(c). Comparing to the valence band spectrum of the powder source (see supporting information S1b), a broad defect band in the band gap centered at a binding energy of 1 eV exists in the as-deposited film. It is interesting to note that there is a very high density of filled states at the Fermi level, indicating electronic behavior similar to a metal. This defect band is probably derived from oxygen vacancies, consistent with the highly sub-stoichiometric MgO_x film composition (i.e., x = 0.75) determined from the core level XPS analysis. Further, Hall effect measurements on the as-deposited MgO_x films show that they behave as an *n*-type semiconductor, with conductivity of 173 S/cm, electron concentration of $\sim 2\times10^{21}$ cm^{-3} and electron mobility of 0.23–0.57 $cm^2V^{-1}s^{-1}$. Interestingly, it has been argued that the enrichment of MgO_x with metallic Mg, which may act as an electron donor species, caused the layer to become an *n*-type semiconductor,[23] in agreement with our observations. The high conductivity of the film revealed by Hall effect is also consistent with the metal-rich composition and the oxygen deficient defect band observed by XPS. Finally, the XPS

Author Manuscript

This article is protected by copyright. All rights reserved.

secondary electron cut-off analysis of a MgO_x/Al stack thinned by sputtering (Argon ion gun, 4keV) illustrated in Figure 1(d) shows a work function in the vicinity of 4.1 eV, which is comparable to the work function of the Al metal itself (~4.2 eV)[24] and to previously measured values of the MgO work function.[25] As will be presented in the next section, the high conductivity and high electron concentration of bulk MgO_x film plays a crucial role in enabling Ohmic contact behavior between the Al electrode and the *n*-type silicon substrates.

To evaluate the electrical contact behaviour of the MgO_x/Al structure, the contact resistivity ρ_c was measured using the method devised by Cox and Strack,[26] as shown schematically in insets of Figure 2(a) and (b), which show a series of *I–V* measurements of samples without and with 1 nm MgO_x interlayer between Al and *n*-type c-Si, respectively. The resistance versus diameter trend is fitted with a spreading resistance model, allowing accurate extraction of ρ_c. As we can see in Figure 2(a), the sample with Al directly on *n*-type c-Si (i.e., without MgO_x) exhibits somewhat Ohmic contacts for large area pads, but then turns to rectifying behaviour when pad areas become smaller. The contact resistance of this particular structure was extracted to be 2 ± 0.5 Ωcm^2. A high contact resistance, or rectifying behavior, between the Al metal and *n*-type c-Si is attributable to the presence of a large surface potential barrier known to exist at this surface.[2] By contrast, the insertion of a nanoscale MgO_x (~1 nm) film improves dramatically the contact behavior, leading to an Ohmic contact (i.e., linear *I–V* curve) between the Al electrode and the *n*-type c-Si substrate. Note that the scale of x-axis (i.e., the voltage) for MgO_x/Al sample is one order magnitude lower than that for samples without MgO_x interlayer. The extracted contact resistance ρ_c for the structure with ~1 nm MgO_x is determined to be 17.5 ± 2 mΩcm^2, which is more than two

Author Manuscript

This article is protected by copyright. All rights reserved.

orders of magnitude lower than the contact of Al directly on *n*-type c-Si. The low resistance for electron transport provided by the MgO_x/Al contact structure is likely attributed to (*i*) a high conductivity and high electron concentration in MgO_x bulk film, as revealed by the Hall effect measurements, and/or (*ii*) the release, or unpinning, of the Fermi-level by passivating the gap states between Al metal and the silicon substrate. It is not anticipated that the work function of MgO_x/Al plays a critical role here in reducing the contact resistivity since its work function is comparable to that of Al metal, as presented in Figure 1(d).

Figure 2(c) presents the effect of MgO_x thickness on contact resistivity. It can be seen that ρ_c first decreases dramatically as the MgO_x thickness increases from 0 to 1 nm, and then increases sharply when MgO_x exceeds 1 nm. The initially decreasing ρ_c could potentially be a result of partial MgO_x surface coverage for the ultra-thin films (for example, less than 1 nm), due to commonly reported island growth for thermal evaporation.[27] The increase in ρ_c for thicker films is likely due to the bulk resistivity of the MgO_x material. It is interesting to note that the contact is still Ohmic even when the MgO_x thickness reaches 60 nm, consistent with the high conductivity and high electron concentration presented above. Nevertheless, it is remarkable that the insertion of ~1 nm thick MgO_x layer results in a contact resistivity of only 17.5 mΩcm^2, promoting an opportunity in fabricating high efficiency silicon solar cells with full-area rear electron contacts. In fact, the contact resistivity stays within tolerable levels for a full area contact up to a MgO_x layer thickness of ~60 nm.

To demonstrate the MgO_x/Al electron contact at the device level, we fabricate a proof-of-concept solar cell with full-area MgO_x /Al stack at the rear surface of an *n*-type silicon wafer. Figure 3(a) depicts the cell schematic structure and Figure 3(b) presents a cross-sectional

This article is protected by copyright. All rights reserved.

transmission electron micrograph of the rear contact layers, respectively. The front (sunward) surface of the cell features (*i*) a textured surface morphology with an array of random upright pyramids to enhance light trapping,[28,29] (*ii*) a boron diffused p^+ region to form a *pn* junction and collect holes, and (*iii*) an alumina / silicon nitride (Al_2O_3/SiN_x) stack to passivate the dangling bonds at the p^+ silicon surfaces and provide antireflection to enhance light coupling into the silicon absorber. The rear surface of cell is coated with a full-area 1 nm MgO_x / 300 nm Al stack. Compared to conventional phosphorus diffused contacts, the MgO_x based contact employed here mitigates the need of (*i*) the high-temperature phosphorus diffusion; and (*ii*) the patterning of the rear dielectrics (by photolithography in many labs, and commonly by laser ablation in industry). Figure 3c provides a photoluminescence image of the front side of a representative solar cell, using a 1025 nm short-pass filter. It shows uniform front and rear surface optics and passivation, and a high excess carrier density over the cell area, which are necessary conditions for a high power conversion efficiency.

The *J–V* photovoltaic characteristic curve under one sun standard illumination is plotted in Figure 3(d) for cells with and without MgO_x interlayer. The electrical parameters of both cells are also tabulated in the inset. The insertion of a 1 nm thick MgO_x layer enhances substantially all cell parameters, leading to a power conversion efficiency of 20%, associated with an open-circuit voltage (V_{OC}), short-circuit current (J_{SC}) and fill factor (*FF*) of 628.8 mV, 39.5 mA/cm^2 and 80.4%, respectively. Compared to the control cell (i.e., without MgO_x interlayer), an absolute 73.6 mV increase of V_{OC} was gained, which is likely attributable to (i) a moderate level of passivation of the rear silicon surface, and/or (ii) the elimination of rectifying contact behavior, both of which are provided by the MgOx/Al stack.

Author Manuscript

This article is protected by copyright. All rights reserved.

We estimate the recombination current density (J_{0c}) under the MgO_x/Al electron-selective contact to be 9.5×10^{-13} A/cm^2 after accounting for 1×10^{-13} A/cm^2 recombination parameter of the front p^+ doped region (composed of 3×10^{-13} A/cm^2 for the metal-contact area and 7×10^{-14} A/cm^2 for the passivated non-contact area) and 5×10^{-14} A/cm^2 for recombination in the bulk of silicon wafer.

Another significant gain in cell performance is the enhancement of *FF* by an absolute 7.1%, which is mainly attributable to the dramatic reduction of the rear contact resistivity, as indicated by R_{series} values in inset of Figure 3(d), consistent with the significant improvement in Ohmic behavior of the contact enabled by the MgO_x interlayer, as presented in Figure 2. The reasonable V_{OC} and high *FF* measured on the cell with a MgO_x/Al contact demonstrate that the latter presents good electron-selective characteristics. Notably, the high *FF* is sustained for a thickness of MgO_x up to 60 nm (see supporting information S2), again consistent with (*i*) the trend of contact resistivity with thickness, and (*ii*) the high conductivity and high electron concentration in the film bulk revealed by Hall effect measurements.

The low J_{SC} of the Al control cell compared to the MgO_x/Al cell is also consistent with a higher recombination loss at the c-Si/Al rear interface compared to the Si/MgO_x/Al interface. An accompanying spectral response analysis is presented in Figure 3(e) for both cells (i.e., with and without MgO_x interlayer). While the reflectance of the two cells is comparable, the insertion of MgO_x interlayer enhances significantly the quantum efficiency (QE) response at long wavelengths (i.e., ~900–1200 nm range). This result indicates again that the MgO_x interlayer provides some passivation of the rear surface of the silicon wafer, consistent with

Author Manuscript

This article is protected by copyright. All rights reserved.

the improvement in V_{OC} and with the lower J_{0c} presented above. Such passivation of interface defects is also consistent with a de-pinning of the Fermi level and a low contact resistivity.

While the MgO_x/Al electron-selective contacts have been demonstrated to enable high efficiency *n*-type c-Si solar cells, the thermal stability of the device remains an important consideration for device longevity and module encapsulation. Cells with 1 nm MgO_x interlayer were annealed in air ambient for 10 minutes at different elevated temperatures in a thermal furnace. Note that the cells for annealing have been fabricated and stored in air for more than two months, exhibiting little change in performance. The resultant cell electrical parameters were plotted in Figure 4 as a function of annealing temperature. As can be seen, the solar cell performance is essentially constant up to 400 °C, and starts deteriorating when temperature increases further. Annealing at 500 °C deteriorated substantially the device performance. The degradation is most likely attributable to the degradation of the MgO_x/Al contact, as evidenced by a significant increase in series resistance, whilst the shunting resistances exhibit little change. We also conducted Hall effect measurements on the 500 °C annealed MgO_x sample, which showed that the conductivity of the film decreased to 2.4×10^{-5} S/cm, which is almost seven orders of magnitude lower than that of the as-deposited MgO_x film. This decrease in conductivity upon annealing is accompanied with a significant increase in film transmittance (see supporting information S3). There are several possible causes for the decrease in conductivity: (i) a reduction of excess metallic Mg upon annealing in air, leading to a more stoichiometric, less conductive material, (ii) a change in the crystallographic structure, evidenced by a change in XRD pattern (see supporting information Figure S4), and (iii) the onset of diffusion of Al through the MgO_x into the *n*-type c-Si, which

Author Manuscript

This article is protected by copyright. All rights reserved.

has been shown to exhibit a rectifying contact. Finally, we also investigated the effect of annealing duration on cell performance by submitting another cell to air-ambient furnace at 400 °C for various lengths of time. As shown in supporting information Figure S5, all cell parameters were stable for annealing times up to 40 minutes. These results demonstrate a great device longevity and sufficient thermal budget for module encapsulation (typically less than 200 °C).

3 Conclusion

This work has demonstrated a novel dopant-free MgO_x/Al electron-selective contact for silicon solar cells. This contact scheme enabled a reduction in contact resistivity by more than two orders of magnitude compared to Al directly deposited on n-type c-Si, which is attributed to a de-pinning (defect passivation) of the Fermi level, together with a high conductivity and high electron concentration in bulk MgO_x film. The 20%-efficient *n*-type c-Si solar cell enabled by these full-area MgO_x/Al electron-selective contacts is remarkable, given the very early proof-of-concept stage of this contact technology. The power conversion efficiency is already comparable to the counterpart *p*-type cells with full-area Al alloyed rear surfaces, which has been achieved after decades of extensive development by world-wide industries and laboratories. The low temperature thin film deposition techniques used in this work, together with the simplified proof-of-concept dopant-free rear contact structure, open up new possibilities in designing and fabricating contact cathodes for organic and/or inorganic optoelectronic devices.

Author Manuscript

This article is protected by copyright. All rights reserved.

4 Experimental section

The structure of MgO_x thin film was studied with X-ray diffraction (XRD). For XRD characterization, thin films of MgO_x were deposited on single side polished c-Si wafers. A PANalytical X'Pert PRO MRD diffractometer with X-ray parabolic mirror and parallel plate collimator (0.27°) was used for the measurements. The diffraction pattern was obtained by using Ni-filtered Cu Kα radiation. A software MDI Jade was applied for analysis of XRD data.

For XPS characterization, thin films of MgO_x/Al were deposited on single-side polished c-Si wafers. A Kratos AXIS Ultra DLD system with a monochromatic Al Kα X-ray source and a hemispherical analyzer was used for the measurements. Secondary electron cut-off and valence band measurements were performed using X-ray excitation, with an added bias to extract the cut-off edge. Work function measurements of the MgO_x/Al interfaces were taken after thinning the Al over–layer thickness to < 5 nm via sputtering. Stoichiometry information was extracted based on fits to the presented core level spectra, and Voigt line-shapes were used for these fits. A Au reference work function at 5.1 eV was measured in the same measurement session, confirming the measurements accuracy.

Hall effect and resistivity measurements were performed with the four contact van der Pauw configeration using Lake Shore 7704A analyser. The contacts constituting of ~50 nm MgO_x and ~300 nm Al layer were fabricated on microscopy glass slab. Current (10 mA for non-annealed, and 1 nA for annealed sample) reversal were used to remove the unwanted thermal electric effects. The magnetic field was kept between 0.1–0.5 T, positive to negative,

Author Manuscript

This article is protected by copyright. All rights reserved.

throughout the measurement to remove the influence of misalignment voltage. All samples were measured in air, under a dark environment, and at room temperature.

The *n*-Si/MgO_x/Al electron-selective contacts were fabricated on planar Czochralski (Cz) *n*-type c-Si wafers with a resistivity of ~1 Ωcm and a thickness of ~250 µm. Samples were subjected to a dilute HF dip prior to evaporation of the contact structures. An array of circular pads with different diameters was evaporated on the front of the test structures via a shadow mask. These pads were deposited as a stack of MgO_x with a variety of thicknesses capped with ~300 nm of Al. A full area Mg (~10 nm) / Al (~300 nm) metal stack was evaporated on the rear surface of the contact samples. Note that Mg thin layer was used here to enhance the Ohmicity of rear contacts reducing the system error in determination of front contact resistivity. Current–voltage (*I–V*) measurements were taken at room temperature using a Keithley 2425 source–meter.

Proof-of-concept cells were fabricated on Cz *n*-type c-Si wafers with a resistivity of ~2.0 Ωcm and a thickness of ~180 µm. The as-cut (100)–oriented silicon wafers were subjected to an alkaline solution of TMAH, deionized water, isopropyl alcohol (IPA) and dissolved silicon at a temperature of 85 °C for 60 minutes, forming textured morphologies with an array of random pyramids.[30-34] After cleaning all samples by the RCA procedure, full–area boron diffusion with sheet resistance of ~120 Ω/□ was then performed in a dedicated clean quartz furnace. The front boron diffused textured surfaces were then passivated with a stack of ~20 nm atomic layer deposited alumina (Al_2O_3) and ~65 nm plasma enhanced chemical vapor deposited silicon nitride (SiN_x). Note that the stack also functions as an antireflection coating. The undiffused rear silicon surfaces were then coated

This article is protected by copyright. All rights reserved.

Author Manuscript

with the novel electron-selective contacts (i.e., ~1 nm MgO_x / 300 nm Al). The front metal grid contact with 10 µm width lines and 1.3 mm pitch was patterned via photolithography, followed by thermal evaporation of a Cr (~10 nm) / Pd(~10 nm) / Ag (~100 nm) stack, and finally thickened by Ag electroplating.

TEM images were acquired from the rear surface of the silicon solar cell that was fabricated per the procedures mentioned above. Cross section of the rear layers was prepared using the focused ion (FIB) beam lift-out technique in a Helios NanoLab 600 DualBeam SEM/FIB system. Final thinning was performed at 5kV and 16pA to reduce FIB induced damage. TEM images were obtained using JEOL 2100F system operating at 200 kV.

The photovoltaic *J–V* behaviour was measured under standard one sun conditions (100 mW/cm^2, AM1.5 spectrum, 25 °C) with a 2 × 2 cm aperture mask using a solar simulator from Sinton Instruments. This simulator was calibrated with a certified Fraunhofer CalLab reference cell. The spectral response measurements were taken using a Protoflex Corporation QE measurement system (QE-1400-03). The reflectance and transmittance were measured using a PerkinElmer Lambda 1050 UV/VIS/NIR spectrophotometer (with an integrating sphere attachment). Photoluminescence (PL) images were taken with a BTimaging LIS-R1 imager using a 1025 nm short-pass filter.

Supporting Information

Supporting Information is available from the Wiley Online Library or from the author.

Acknowledgments

Author Manuscript

This article is protected by copyright. All rights reserved.

This work was supported by the Australian Government through the Australian Research Council (Discovery Project: DP150104331). Some facilities at the Australian National Fabrication Facility and Centre for Advanced Microscopy at ANU were used. XPS characterization was performed at the Joint Center for Artificial Photosynthesis, supported through the Office of Science of the US Department of Energy under Award Number DE-SC0004993. AJ, MH and JB acknowledge funding from the Bay Area Photovoltaics Consortium (BAPVC).

Author Manuscript

[1] Dieter K. Schroder, *Semiconductor material and device characterization*, 3rd ed. (John Wiley & Sons Inc., Hoboken, New Jersey, USA, **2006**).

[2] S. M. Sze and K. K. Ng, *Physics of Semiconductor Devices*. (John Wiley & Sons, **2006**).

[3] Jianhua Zhao, Solar Energy Materials and Solar Cells 82 (1-2), 53 (**2004**).

[4] SW Glunz, F Feldmann, A Richter, M Bivour, C Reichel, H Steinkemper, J Benick, and M Hermle, presented at the 31st European Photovoltaic Solar Energy Conference and Exhibition, Hamburg, Germany, **2015**.

[5] K. Masuko, M. Shigematsu, T. Hashiguchi, D. Fujishima, M. Kai, N. Yoshimura, T. Yamaguchi, Y. Ichihashi, T. Mishima, N. Matsubara, T. Yamanishi, T. Takahama, M. Taguchi, E. Maruyama, and S. Okamoto, Photovoltaics, IEEE Journal of 4 (6), 1433 (**2014**).

[6] Thomas G. Allen, Peiting Zheng, Ben Vaughan, Matthew Barr, Yimao Wan, Christian Samundsett, James Bullock, and Andres Cuevas1, presented at the IEEE 43rd Photovoltaic Specialists Conference (PVSC), Portland, OR, **2016**.

[7] P. L. Janega, J. McCaffrey, D. Landheer, M. Buchanan, M. Denhoff, and D. Mitchel, Applied Physics Letters 53 (21), 2056 (**1988**).

[8] Jerzy Kanicki, Applied Physics Letters 53 (20), 1943 (**1988**).

[9] Masahiro Akiya and Hiroaki Nakamura, Journal of Applied Physics 59 (5), 1596 (**1986**).

[10] Yimao Wan, Chris Samundsett, Di Yan, Thomas Allen, Jun Peng, Jie Cui, Xinyu Zhang, James Bullock, and Andres Cuevas, Submitted (**2016**).

[11] Yunfang Zhang, Ruiyuan Liu, Shuit-Tong Lee, and Baoquan Sun, Applied Physics Letters 104 (8), 083514 (**2014**).

This article is protected by copyright. All rights reserved.

[12] J. Bullock, M. Hettick, J. Geissbühler, A. J. Ong, T. Allen, C. M. Sutter-Fella, T. Chen, H. Ota, E. W. Schaler, S. De Wolf, C. Ballif, A. Cuevas, and A. Javey, Nature Energy 1 (15031) (**2016**).

[13] James Bullock, Peiting Zheng, Quentin Jeangros, Mahmut Tosun, Mark Hettick, Carolin M Sutter‐Fella, Yimao Wan, Thomas Allen, Di Yan, and Daniel Macdonald, Advanced Energy Materials (**2016**).

[14] Yimao Wan, Christian Samundsett, James Bullock, Thomas Allen, Mark Hettick, Di Yan, Peiting Zheng, Xinyu Zhang, Jie Cui, and Josephine Anne McKeon, ACS applied materials & interfaces (**2016**).

[15] Yunfang Zhang, Wei Cui, Yawen Zhu, Fengshuo Zu, Liangsheng Liao, Shuit-Tong Lee, and Baoquan Sun, Energy & Environmental Science 8 (1), 297 (**2015**).

[16] James Bullock, Yimao Wan, Mark Hettick, Jonas Geissbühler, Alison J. Ong, Daisuke Kiriya, Di Yan, Thomas Allen, Jun Peng, Zhang Xinyu, Carolin M. Sutter-Fella, Stefaan De Wolf Christophe Ballif, Andrés Cuevas, and Ali Javey, presented at the IEEE 43rd Photovoltaic Specialist Conference (PVSC), Portland, Oregon, **2016**.

[17] Sushobhan Avasthi, William E. McClain, Gabriel Man, Antoine Kahn, Jeffrey Schwartz, and James C. Sturm, Applied Physics Letters 102 (20) (**2013**).

[18] Xinbo Yang, Peiting Zheng, Qunyu Bi, and Klaus Weber, Solar Energy Materials and Solar Cells 150, 32 (**2016**).

[19] Ho Won Choi, Soo Young Kim, Woong-Kwon Kim, and Jong-Lam Lee, Applied Physics Letters 87 (8), 082102 (**2005**).

[20] O. E. Taurian, M. Springborg, and N. E. Christensen, Solid State Communications 55 (4), 351 (**1985**).

[21] Gill Sang Han, Hyun Suk Chung, Byeong Jo Kim, Dong Hoe Kim, Jin Wook Lee, Bhabani Sankar Swain, Khalid Mahmood, Jin Sun Yoo, Nam-Gyu Park, Jung Heon Lee, and Hyun Suk Jung, Journal of Materials Chemistry A 3 (17), 9160 (**2015**).

[22] Ashish Kulkarni, Ajay K. Jena, Hsin-Wei Chen, Yoshitaka Sanehira, Masashi Ikegami, and Tsutomu Miyasaka, Solar Energy 136, 379 (**2016**).

[23] Jason S. Corneille, Jian-Wei He, and D. Wayne Goodman, Surface Science 306 (3), 269 (**1994**).

Author Manuscript

This article is protected by copyright. All rights reserved.

[24] Gregory N. Derry, Megan E. Kern, and Eli H. Worth, Journal of Vacuum Science & Technology A 33 (6), 060801 (**2015**).

[25] Jae Yong Lim, Jun Soek Oh, Byung Doc Ko, Jae Won Cho, Seung Oun Kang, Guangsup Cho, Han Sup Uhm, and Eun Ha Choi, Journal of Applied Physics 94 (1), 764 (**2003**).

[26] R. H. Cox and H. Strack, Solid-State Electronics 10 (12), 1213 (**1967**).

[27] Furong Zhu, Beeling Low, Keran Zhang, and Soojin Chua, Applied Physics Letters 79 (8), 1205 (**2001**).

[28] Patrick Campbell and Martin A. Green, Journal of Applied Physics 62 (1), 243 (**1987**).

[29] Patrick Campbell and Martin A. Green, Solar Energy Materials and Solar Cells 65 (1–4), 369 (**2001**).

[30] M. G. Coleman W. L. Bailey, C. B. Harris, and I. A. Lesk, U.S. Patent No. 4137123 (**Jan. 30, 1979**).

[31] Osamu Tabata, Ryouji Asahi, Hirofumi Funabashi, Keiichi Shimaoka, and Susumu Sugiyama, Sensors and Actuators A: Physical 34 (1), 51 (**1992**).

[32] L. M. Landsberger, S. Naseh, M. Kahrizi, and M. Paranjape, Microelectromechanical Systems, Journal of 5 (2), 106 (**1996**).

[33] Jae Sung You, Donghwan Kim, Joo Youl Huh, Ho Joon Park, James Jungho Pak, and Choon Sik Kang, Solar Energy Materials and Solar Cells 66 (1–4), 37 (**2001**).

[34] P. Papet, O. Nichiporuk, A. Kaminski, Y. Rozier, J. Kraiem, J. F. Lelievre, A. Chaumartin, A. Fave, and M. Lemiti, Solar Energy Materials and Solar Cells 90 (15), 2319 (**2006**).

Author Manuscript

This article is protected by copyright. All rights reserved.

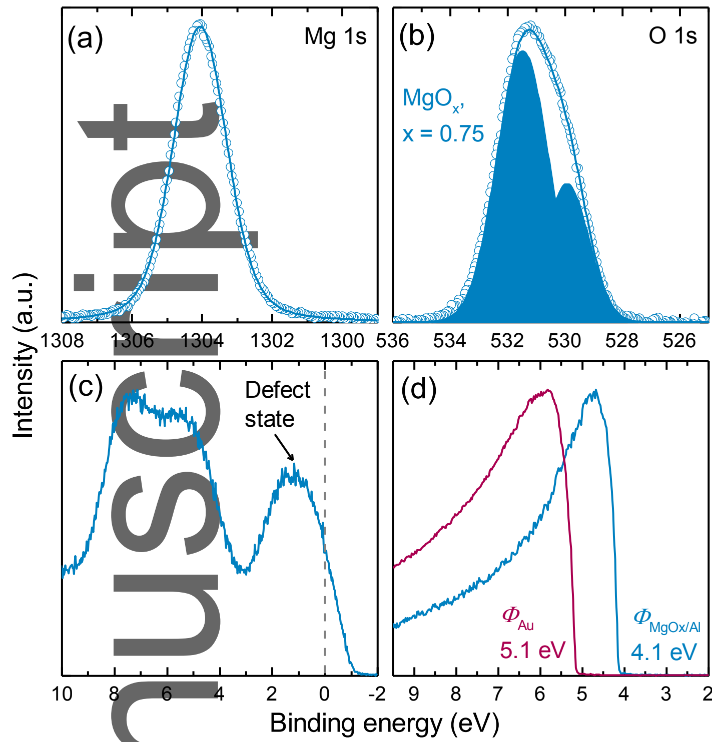

Figure 1: X-ray photoelectron spectroscopy (XPS) measurements of thermally evaporated MgO_x films. (a) and (b) present the core level spectrum of Mg 1s and O 1s, respectively. The extracted stoichiometry of MgO_x is also included. (c) shows the valence band spectrum of the MgO_x film. (d) shows the secondary electron cut-off spectrum measured at the MgO_x/Al interface with a gold (Au) reference.

Author Manuscript

This article is protected by copyright. All rights reserved.

Author Manuscript

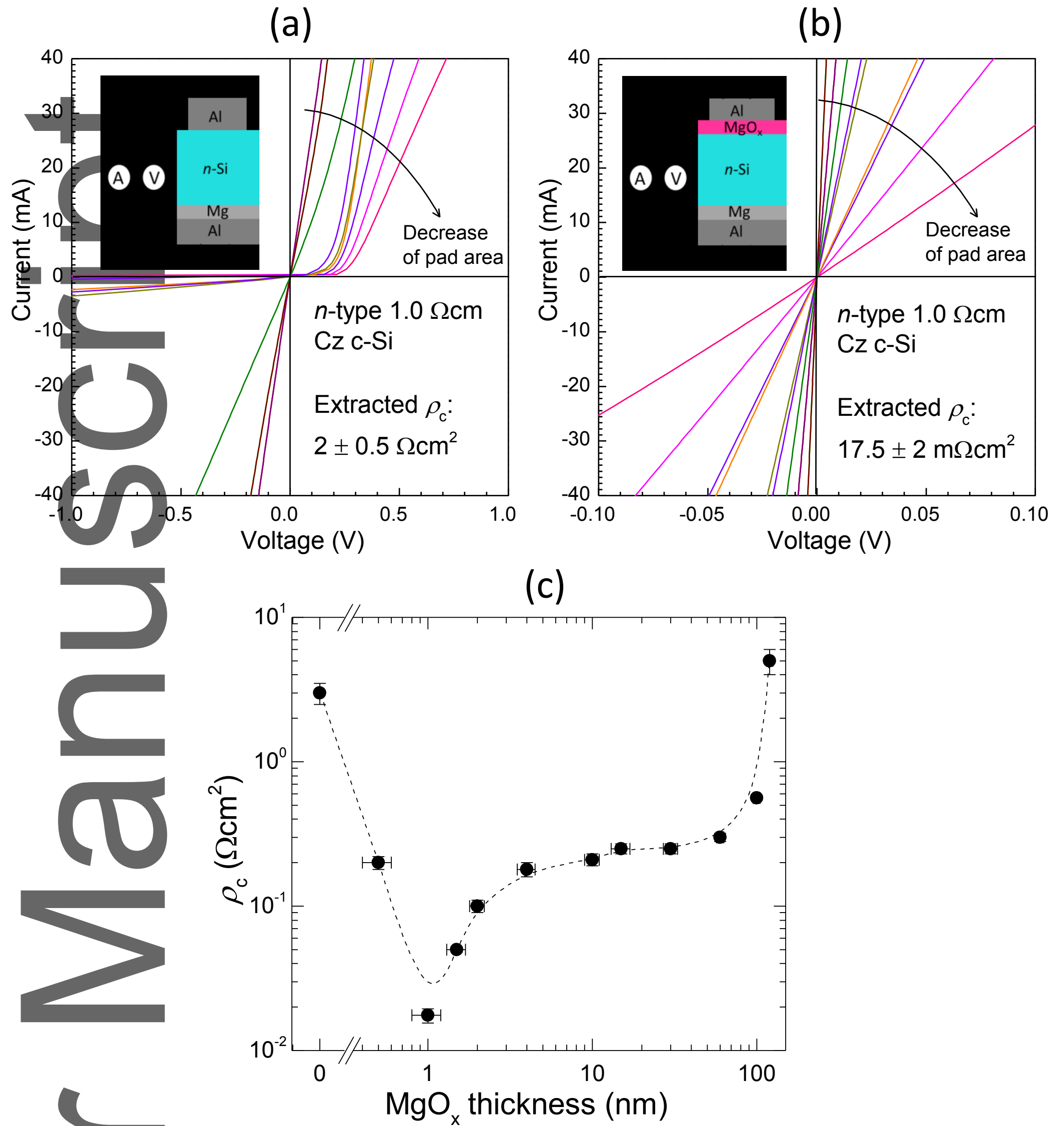

Figure 2: Contact resistivity measurements of MgO_x based contacts to *n*-type c-Si. (a) and (b) present a series of *I–V* measurements of samples without and with 1 nm MgO_x interlayer between Al and *n*-type c-Si, respectively. Schematics of the contact resistivity test structure for both samples are included in respective inset. (c) shows the contact resistivity ρ_c as a function of MgO_x thickness.

This article is protected by copyright. All rights reserved.

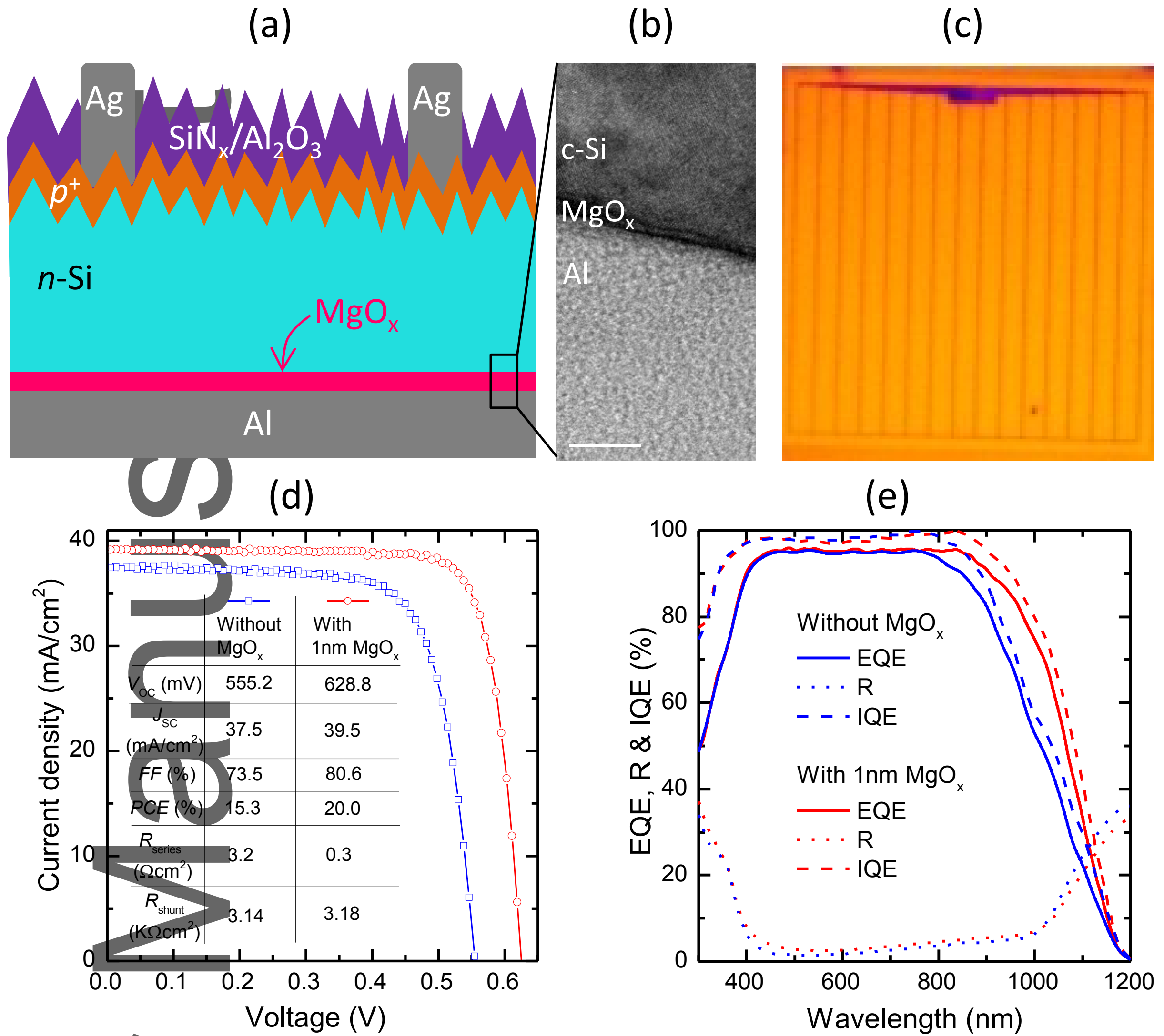

Figure 3: Device results with full-area rear MgO_x based electron-selective contacts. (a) illustrates the schematic of an *n*-type silicon solar cell featuring full-area rear MgO_x/Al electron-selective contacts. (b) presents the 10 nm scale cross-sectional transmission electron micrograph (TEM) of the rear layers of the cell. (c) shows photoluminescence image of the front (sunward) side of a representative solar cell, using a 1025 nm short-pass filter. (d) presents the light *J–V* behavior and electrical parameters of the cell measured under standard one sun conditions for cells without and with ~1 nm MgO_x interlayer. (e) shows the external and internal quantum efficiencies accompanied the measured reflectance for the two cells.

Author Manuscript

This article is protected by copyright. All rights reserved.

Author Manuscript

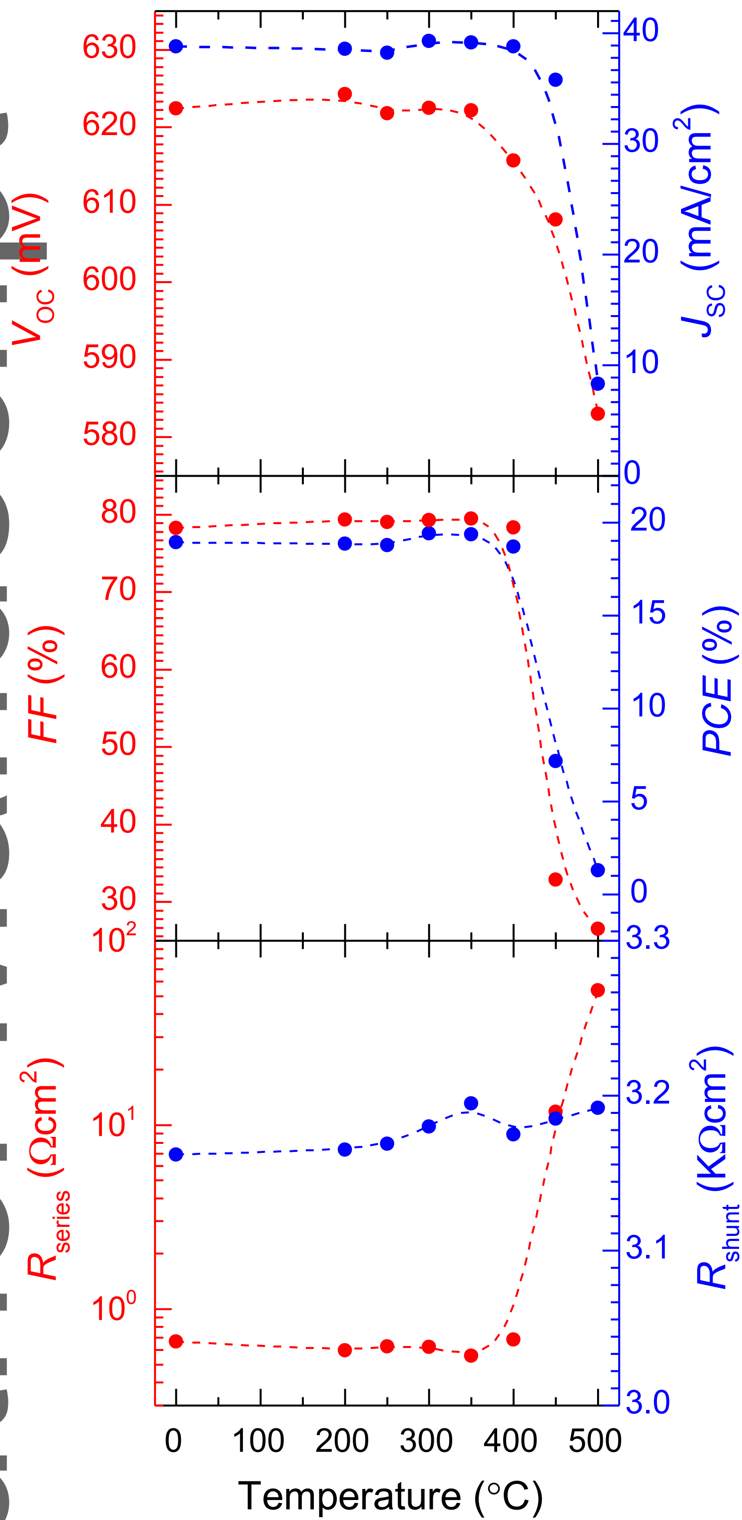

Figure 4: Thermal stability of the devices. Electrical parameters (V_{OC}, J_{SC}, FF, PCE, R_{series} and R_{shunt}) as function of annealing temperature in thermal furnace air ambient for 10 minutes.

This article is protected by copyright. All rights reserved.

A highly conductive and thermally stable electrode composed of a nanoscale magnesium oxide / aluminium (MgO_x/Al) contact is demonstrated to achieve moderately low resistivity Ohmic contacts on lightly doped *n*-type c-Si. A power conversion efficiency of 20% is obtained at a proof-of-concept stage of *n*-type c-Si solar cells with full-area MgO_x/Al rear contacts.

Keywords: solar cell, magnesium oxide, electron-selective contact

Yimao Wan, Chris Samundsett, James Bullock, Mark Hettick, Thomas Allen, Di Yan, Jun Peng, Yiliang Wu, Jie Cui, Ali Javey, and Andres Cuevas*

Conductive and Stable Magnesium Oxide Electron-Selective Contacts for Efficient Silicon Solar Cells

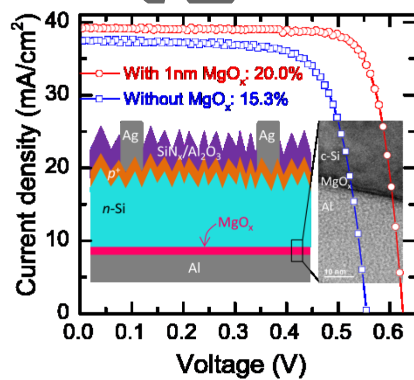

Author Manuscript

This article is protected by copyright. All rights reserved.